Crack monitoring in reinforced concrete beams by distributed optical fiber sensors

STRUCTURE AND INFRASTRUCTURE ENGINEERING
2021, VOL. 17, NO. 1, 124–139
https://doi.org/10.1080/15732479.2020.1731558

Crack monitoring in reinforced concrete beams by distributed optical fiber sensors

Carlos G. Berrocal[a,b], Ignasi Fernandez[a] and Rasmus Rempling[a,c]

[a]Division of Structural Engineering, Chalmers University of Technology, Göteborg, Sweden; [b]Thomas Concrete Group AB, Göteborg, Sweden; [c]NCC Sverige AB, Göteborg, Sweden

ABSTRACT

This paper investigates the use of distributed optical fiber sensors (DOFS) based on Optical Frequency Domain Reflectometry of Rayleigh backscattering for Structural Health Monitoring purposes in civil engineering structures. More specifically, the results of a series of laboratory experiments aimed at assessing the suitability and accuracy of DOFS for crack monitoring in reinforced concrete members subjected to external loading are reported. The experiments consisted on three-point bending tests of concrete beams, where a polyamide-coated optical fiber sensor was bonded directly onto the surface of an unaltered reinforcement bar and protected by a layer of silicone. The strain measurements obtained by the DOFS system exhibited an accuracy equivalent to that provided by traditional electrical foil gauges. Moreover, the analysis of the high spatial resolution strain profiles provided by the DOFS enabled the effective detection of crack formation. Furthermore, the comparison of the reinforcement strain profiles with measurements from a digital image correlation system revealed that determining the location of cracks and tracking the evolution of the crack width over time were both feasible, with most errors being below ±3 cm and ±20 μm, for the crack location and crack width, respectively.

ARTICLE HISTORY
Received 21 July 2019
Revised 26 October 2019
Accepted 22 November 2019

KEYWORDS
Concrete beams; crack monitoring; damage assessment; distributed optical fiber sensors; reinforced concrete; structural health monitoring

1. Introduction

The use of an effective Structural Health Monitoring (SHM) system could enable the early detection of deficiencies in civil engineering structures and aid engineers and infrastructure owners in making informed decisions, thereby leading to well-planned, timely maintenance operations with minimal disruption to the users and the consequent substantial savings in terms of both money and time. However, despite the great efforts made in the research and development of SHM systems, see e.g. (Cawley, 2018; Seo, Hu, & Lee, 2016), due to the lack of reliable, scalable and affordable monitoring solutions, SHM is not yet implemented as a standard practice in most civil engineering structures (Glišić, Hubbell, Sigurdardottir, & Yao, 2013).

One of the main elements in SHM systems is the sensing devices. Traditional SHM systems have often relied on relatively large, electrically powered sensors, such as displacement transducers, inclinometers, accelerometers, etc. However, over the last decades, the use of optical fiber sensors in the field of SHM for strain and temperature monitoring has gained popularity owing to several features that makes them very suitable for SHM applications. Optical fibers can be easily bonded or embedded into a structure thanks to their reduced dimensions (often $<200\,\mu m$ in diameter), they are lightweight which facilitates their transport and handling, they are chemically inert, corrosion resistant and able to operate over a wide range of temperatures, thus being suitable for a variety of environments and unlike electrically powered sensors, optical fibers are not affected by electromagnetic interference (EMI) caused by nearby electromagnetic field sources. More importantly, a single optical fiber can accommodate multiple sensing points along its length, thereby saving tremendous amounts of time and money in wiring and installation (Casas & Cruz, 2003).

Among the existing types of fiber optical measurement, those based on Fiber Bragg Grating (FBG) have received a great deal of attention in the past, see e.g. (Davis, Bellemore, & Kersey, 1997; Morey, Dunphy, & Meltz, 1992) and to date they are the most widely used system (Barrias, Casas, & Villalba, 2016). The principle of FBG systems is based on the modification of the refractive index inside the fiber core by creating a periodic pattern that selectively reflects a specific wavelength (Todd, Johnson, & Vohra, 2001). Using wavelength division multiplexing, multiple points along the fiber can be measured, yet this system presents certain limitations with respect to spatial resolution and number of sensing points per fiber, hence it is regarded as a discrete or quasi-distributed system (Majumder, Gangopadhyay, Chakraborty, Dasgupta, & Bhattacharya, 2008). Consequently, even though FBG systems can provide useful information about the global behaviour of a structure and the local behaviour at specific locations, they fall short of providing a truly continuous description of the strain

CONTACT Carlos G. Berrocal carlos.gil@chalmers.se Division of Structural Engineering, Chalmers University of Technology, Göteborg, Sweden

variation along the structure, which can be a critical issue in certain cases, e.g. for crack monitoring in concrete structures, where the exact location of cracks cannot be a priori determined.

Distributed Optical Fiber Sensors (DOFS), on the other hand, measure the return loss of the emitted light caused by the backscattering that occurs along the fiber due to different phenomena. Accordingly, DOFS do not require the alteration of the fiber core since every segment in the fiber acts as a sensor, thereby achieving a significant improvement in spatial resolution compared to FBG systems. There are three different scattering phenomena occurring concurrently that can be used to measure variations of temperature and/or strain along the fiber: Raman, Brillouin and Rayleigh scattering (Soga & Luo, 2018).

Raman scattering arises from the thermal vibration of the glass molecules in the fiber core as light travels through the fiber and is highly sensitive to temperature variations (Rodriguez, Casas, & Villalba, 2015b). Brillouin scattering is produced by the interaction of backscattered light and acoustic waves generated when changes in the density of the material occur as a result of thermal effects. Brillouin scattering is sensitive to external changes of both mechanical strain and temperature and despite its measuring range can reach lengths of up to more than 300 km (Gyger, Rochat, Chin, Niklès, & Thévenaz, 2014), the spatial resolution that can be achieved is often limited to several centimetres (Güemes, Fernández-López, & Soller, 2010). Rayleigh scattering, on the other hand, refers to the elastic distribution of light in all directions that happens when light interferes with local inhomogeneities in the fiber core that are smaller than the wavelength of the light itself. These inhomogeneities are caused by fluctuations in the density and composition of the fiber core, which makes Rayleigh scattering sensitive to both mechanical strain and temperature changes (Palmieri, 2013). Systems based on Rayleigh scattering are currently limited to a measuring range of up to 2 km, but in exchange they provide an unprecedented spatial resolution that can go down to the the sub-millimetric scale, thereby offering new possibilities for the development of damage detection systems (Rodriguez et al., 2015b).

Rayleigh scattering analysis is based on Optical Frequency Domain Reflectometry (OFDR) where the Rayleigh scattering pattern occurring along the fiber is initially measured and stored as a fingerprint or signature of the fiber in a reference state. The Rayleigh scattering profile is measured again when the fiber is subjected to mechanical strain or temperature perturbations and subsequently both data sets are divided into small segments that are Fourier transformed into the frequency domain. By performing a cross-correlation operation between the reference and perturbed states, a spectral shift in the correlation peak can be found which can be then calibrated to strain or temperature changes (Ding et al., 2018). The principle of OFDR of Rayleigh backscattering is illustrated in Figure 1.

The clear advantages of optical fiber sensors have attracted the interest of many researchers over the years. As a result, the suitability of optical fiber systems in SHM has already been tested for various experiments in the laboratory, see e.g. (Bado, Casas, & Barrias, 2018; Bao, Meng, Chen, Chen, & Khayat, 2015; Sienko, Bednarski, & Howiacki, 2019; Zeng et al., 2002), as well as field applications, see e.g. (Barrias, Rodriguez, Casas, & Villalba, 2018; Brault, Hoult, Greenough, & Trudeau, 2019; Glišić, Posenato, & Inaudi, 2007; Matta, Bastianini, Galati, Casadei, & Nanni, 2008). In the case of reinforced concrete structures, several authors have reported successful results in detecting the onset and the location of load-induced cracking, both for fibers with protective coatings commonly embedded in the concrete, see e.g. (Bao & Chen, 2015; Henault et al., 2012; Imai et al., 2010) as well as for fibers without any intermediate layer between the fiber and the substrate, frequently attached to the surface of the hardened concrete, see e.g. (Davis, Hoult, Bajaj, & Bentz, 2017; Regier & Hoult, 2015; Rodriguez, Casas, & Villalba, 2015a).

Despite the advances in crack monitoring techniques based on DOFS measurements, one of the remaining challenges is to achieve accurate predictions of crack widths in reinforced concrete members. For optical fiber sensors with a series of intermediate layers (outer claddings, coatings, sheaths, jacketing, etc.) between the fiber core and the host material, due to the lower stiffness of the intermediate layers, the transfer of localized strains in the substrate results in fiber strains smeared over a certain distance of up to several centimetres. Feng, Zhou, Sun, Zhang, and Ansari (2013), formulated a mechanical model based on shear lag theory to evaluate the relationship between strain discontinuities, such as cracks, and the measured strain distribution in optical fiber sensors. This model has been later applied by others to predict the surface crack width of concrete structures by DOFS bonded to the surface of the concrete (Billon et al., 2015) as well as embedded in the concrete (Bassil et al., 2019). While promising results have been reported, the proposed model requires the calibration of the shear lag factor, which depends on the material and geometrical properties of the cables, and it is not directly applicable to fiber sensors bonded to the reinforcement, where the assumption of perfect bond between all layers is not fulfilled.

Recent work carried out by the groups of Prof. Casas and Prof. Hoult, have both shown great progress in the quantification of crack widths in RC structures using Rayleigh-based DOFS bonded without intermediate layers between optical fiber sensor and the host material. In (Rodriguez et al., 2015a), a methodology for the location and quantification of crack widths is presented based on strain measurements from a DOFS bonded to the tension surface of a concrete element. Their method was evaluated experimentally using crack measurements obtained by magnetic transducers from a RC slab tested in bending up to failure and further validated with nonlinear finite element modelling. A similar approach was used in (Rodriguez, Casas, & Villalba, 2019) to quantify the width of shear cracks, where the authors bonded DOFS on the surface of the web of three concrete beams to create a two-dimensional grid of fiber sensors able to measure strain profiles in two orthogonal directions. In both studies the crack width estimations obtained by their

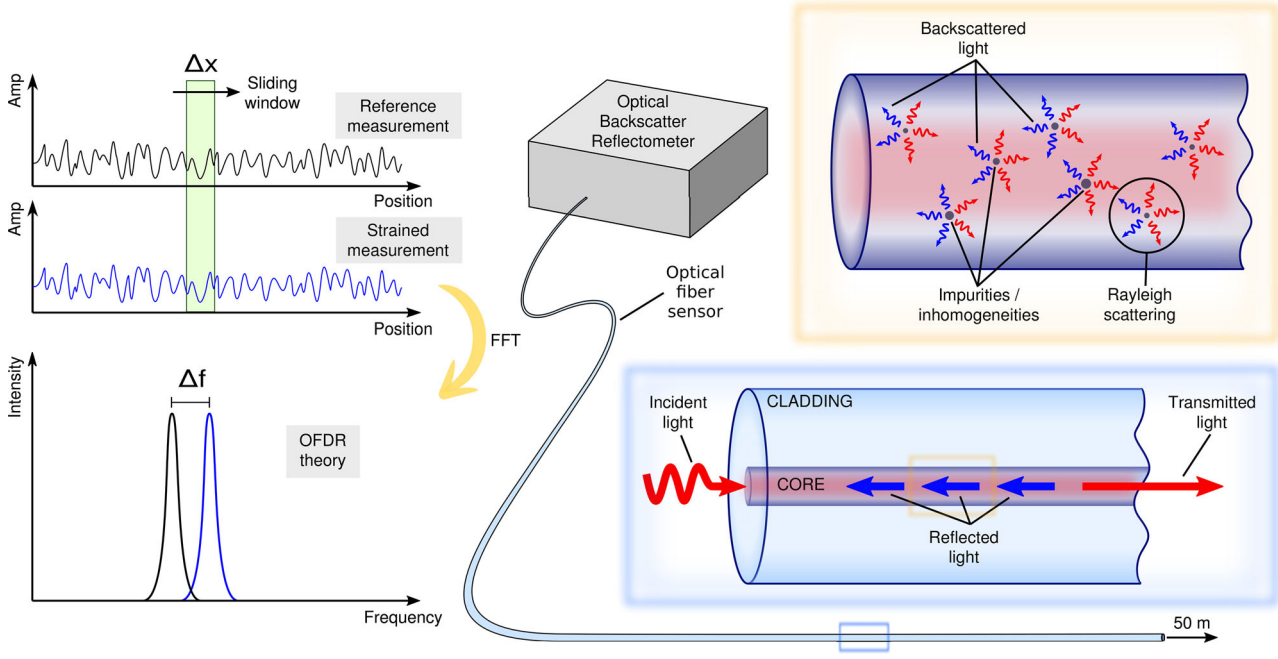

Figure 1. Working principle of Rayleigh Backscattering optical fiber sensors based on OFDR.

method based on the strain profiles measured by the DOFS compared well with the crack width measurements from transducers. However, one of the limitations of their method is that it only provides an average crack width over the cracked region.

In a recent piece of work by (Brault & Hoult, 2019b), the authors investigated the feasibility of using of DOFS bonded to the surface of concrete to evaluate the deflection and cracking of reinforced concrete beams subjected to three-point bending. Unlike in previous studies, their method enabled the quantification of individual cracks, which showed good agreement with experimental crack width measurements obtained by Digital Image Correlation (DIC) technique. In another study by (Brault & Hoult, 2019a), the authors tested the ability of two different types of fiber sensors, namely nylon-coated and polyamide-coated, to locate cracks when the DOFS are bonded to the reinforcement and investigated the relationship between surface crack widths, as measured by DIC, and the reinforcement strain at the cracks as measured by the DOFS. In both studies, the authors showed very promising results and the great potential of DOFS for crack monitoring in RC structures.

The aim of the present study was to explore the feasibility of obtaining quantitative crack-damage information through the monitoring of strain distributions by optical fiber sensors directly bonded to the reinforcement. This article reports the findings from laboratory experiments aimed at validating the suitability of Rayleigh scattering based DOFS glued to steel reinforcement to detect crack formation and determine crack location as reported by others (cf. Brault & Hoult, 2019a). Additionally, a new method to estimate crack widths in reinforced concrete beams subjected to external loading is proposed. To that end, electrical strain gauges and Digital Image Correlation (DIC) were used in combination with optical fiber sensors to explore the accuracy and reliability of DOFS under monotonic and cyclic loading as well as to test the ability of the proposed method to estimate crack widths.

2. Description of experiments

The main objective of this study was to explore whether strain measurements from Rayleigh scattering DOFS, which have been rendered very promising for the detection of crack formation in reinforced concrete structures, could be also used to obtain quantitative information about the extent of cracking when bonded to the reinforcement. For that purpose, an experimental program comprising a total of eight reinforced concrete beams was devised. Two of the beams, which were used as reference specimens to validate the predicted failure mode and ultimate load, were not instrumented with optical fiber sensors, hence their results are not presented. The remaining six beams were measured using electrical strain foil gauges, optical fiber sensors and DIC. Two of the measured beams were loaded monotonically up to failure whereas four were subjected to cyclic loading. In the following, the most relevant details about the experimental programme are summarised.

2.1. Specimen geometry

In the present study, beam specimens with dimensions of 900 mm in length and a cross-section of 100×150 mm were designed to monitor the cracking process. Each beam was reinforced with two ∅10 mm rebar of normal ductility carbon-steel (B500B). The rebars were supported on spacers placed at the corners of the forms to ensure a clear concrete cover of 25 mm between rebars and the bottom and side surfaces of the forms. The ends of the bars were bent upwards to provide better anchorage as well as to create a

safe way out for the optical fiber sensors. Moreover, no stirrups were placed to ensure the beams underwent shear failure, based on the requirements of a parallel study where the same beams were used. The geometry and reinforcement layout of the beam specimens are depicted in Figure 2.

2.2. Materials and sample preparation

All beams were cast in playwood forms with a concrete mix featuring a water-to-cement ratio (*w/c*) of 0.45 and prepared using a Portland cement with low C_3A content and moderate heat development. In order to minimise the risk of accidentally damaging the sensors during casting, a self-compacting mix was designed to remove the need of compaction and vibration of the concrete. The mix proportions are given in Table 1. After casting, the beam specimens were covered with a polyethylene sheet to prevent moisture evaporation and they were stored to cure in the forms in an indoor climate ($20 \pm 2\,^{\circ}C$ and $60 \pm 5\%$ RH) for 40 days prior to testing.

Material tests were also carried out to assess the mechanical properties of the concrete and the steel reinforcement. The concrete compressive strength was assessed in accordance with EN 12390-3,3 (2009) using three 100 mm cubes while splitting tensile strength tests were conducted on three 150 mm cubes in accordance with EN 12390-6,6 (2001). The mechanical properties of the steel reinforcement were determined through tensile tests according to EN ISO 15630-1 (2019). The results from the material tests are summarised in Table 2.

2.3. Sensor installation and strain monitoring

Three different systems were used to measure strains in the beam during the bending tests, namely electrical foil strain gauges, distributed optical fiber sensors and DIC. The electrical strain gauges were 3 mm foil gauges from HBM used in a quarter bridge configuration. The foil gauges were placed at the centre of one of the rebars in each of the beams using a two-component epoxy resin adhesive (see Figure 2). It must be noted that to provide a sufficiently large flat surface suitable to accommodate the foil gauge in the rebar, one of the transverse ribs was ground down. The sampling rate for the foil gauges was set to obtain 1000 measurements per hour, hence ~3.6 Hz.

Different configurations to deploy optical fiber sensors in reinforced concrete have been described in the literature, such as attaching the fiber to the concrete surface (Brault & Hoult, 2019b; Grzymski, Trapko, & Musiał, 2019), embedding a jacketed fiber into the concrete (Henault et al., 2012) or attaching the fiber to the reinforcement either by bonding it to the surface (Barrias, Casas, & Villalba, 2017; Brault & Hoult, 2019b) or inserting it into a previously etched groove (Du et al., 2018; Kaklauskas, Sokolov, Ramanauskas, & Jakubovskis, 2019). For crack detection purposes, bonding the fiber directly onto the concrete surface is intuitively the best choice, since large strain concentrations induced by the crack formation can be easily detectable. Loss of information after cracking, however, may occur if the strains in the fiber exceed its measuring range when uncoated fibers are used in combination with stiff adhesives, which highlights the importance of choosing and correctly applying the right adhesive so that stresses are properly transferred from the substrate material to the fiber core, cf. (Barrias, Casas, & Villalba, 2019a). Attaching the fiber to the reinforcement, on the other hand, may not only be used to assess the cracking state of the structures but it can also provide valuable information about the loading state. However, attaching the optical fiber sensors to the reinforcement limits their application to newly built structures.

In this study, the optical fiber sensors used (polyimide coated low-bend loss fibers with a 155 µm diameter) were attached directly onto the rebar along one of the longitudinal ridges (see Figure 2). The rebars were sand-blasted and degreased with acetone prior to the installation of the fiber. The bonding of the fiber was achieved by applying a thin layer of cyanoacrylate adhesive, which according to the literature, exhibits a better performance than two-component epoxy adhesives commonly used to attach foil strain gauges (Barrias, Casas, & Villalba, 2018). Another important documented issue related to the use of unprotected DOFS embedded in concrete is the appearance of anomalous strain readings after concrete cracking, see e.g. (Barrias, Rodriguez, et al., 2018; Regier & Hoult, 2015). Consequently, an abundant layer of a one-component water-proof silicone rubber material was applied for protection based on the findings by (Davis et al., 2017). It should be noted that foil gauges and optical fibers were installed in different rebars. The Optical Distributed Sensor Interrogator (ODiSI) 6000 series from Luna Inc. was used as interrogation unit. The spatial resolution in the fiber sensor was 0.625 mm between measuring points while the sample rate was 5 Hz.

Furthermore, the measurement of full-field deformation and strains of one of the lateral sides of the beams was performed on all the elements tested. For that purpose, the commercially available optical deformation measurement system from GOM, ARAMIS®, was employed. The system relies on a non-contact measurement technique based on Digital Image Correlation (DIC) with an adjustable stereo-camera setup, consisting of two CCD cameras with 12.0 Megapixel resolution (4000×3000 pixels). The cameras were mounted on a rigid bar specifically designed for the purpose with an angle of 25.5° while the separation of the cameras and the distance to the beam were adjusted according to the prescribed measuring volume. In this study the system was calibrated for a measurement volume of $980 \times 795 \times 795\,mm^3$, hence covering the full length of the specimen. The calibration information indicated a deviation of 0.035 pixel which, considering the camera resolution and measured length, provided an accuracy of 8.5 µm.

The main purpose of the use of DIC was to obtain accurate and reliable information about the formation and development of cracks. Additionally, DIC measurements were also used to compute the deflection of the beams, where the settlement over the supports was subtracted from the vertical displacement at the mid-span. The sample rate used for the DIC was lower than for the embedded sensors at only

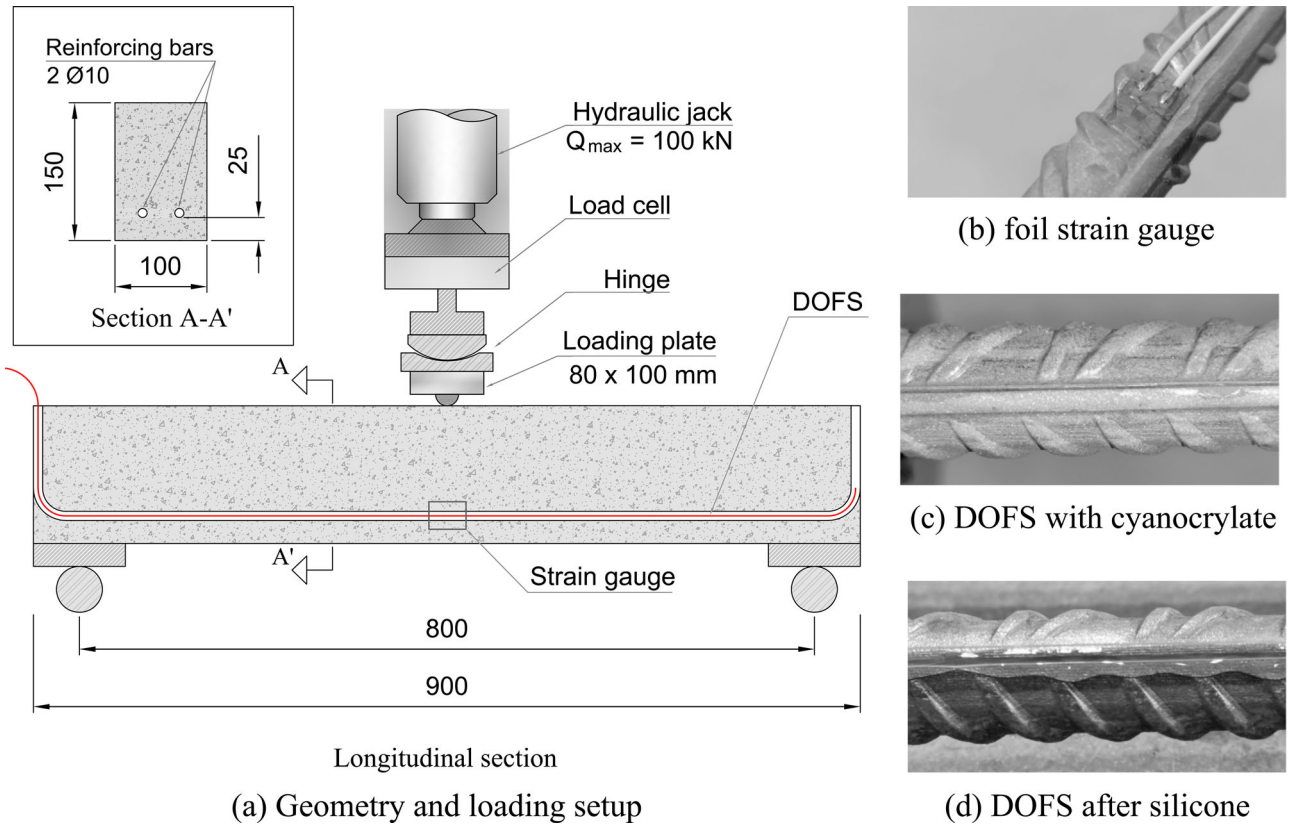

Figure 2. (a) Beam geometry, reinforcement layout and loading setup (all measurements in mm); (b) foil strain gauge installed a rebar with one of the ribs previously removed; (c) polyamide coated DOFS bonded along the longitudinal ridge of a rebar with cyanoacrylate adhesive; (d) Installed DOFS after the application of a protective layer of silicone.

Table 1. Concrete mix proportions, in kg/m^3.

Component	Dosage
Cement (CEM I 42.5N BV/SR/LA)	415
Limestone filler (Limus 40)	75
Fine aggregate (sand 0/4)	868,3
Coarse aggregate (crushed 5/8)	862
Effective water	186,8
Superplasticizer – Glenium 51/18	6,64

Table 2. Material properties.

Concrete		
Property	Average	COV (%)
Compressive strength at 28 days [MPa]	59	1
Compressive strength at testing (40 days) [MPa]	61	2
Splitting tensile strength at 28 days [MPa]	4	5.5
Steel reinforcement		
Property	Average	COV (%)
Yield strength [MPa]	518	3.3
Ultimate strength [MPa]	628	4.5
Elastic Modulus [GPa]	200	6.2

0.2 Hz. It is worthwhile mentioning that relative position of the rebars with the foil gauge and the fiber sensor was varied, so that the rebar with the optical fiber sensor was in some cases closest to the surface of the beam monitored with DIC and sometimes further away.

2.4. Loading setup

In order to induce cracking, the beam specimens were simply supported on rollers and loaded under a three-point bending setup. The distance between the centre of the supports was equal to 800 mm and the point load was applied at mid-span, thus leaving a shear span of 400 mm. The loading setup is schematically illustrated in Figure 2. Loading was applied under displacement control using a closed-loop feedback system at a displacement rate of 0.5 mm/min. Two different loading schemes were used in the tests, monotonic loading up until failure and cyclic loading with gradually increasing load levels.

3. Results and discussion

All of the tested beams presented very similar results in terms of structural performance with consistent values of the maximum load and deflection achieved prior to failure as well as a similar number of cracks formed, see Table 3. Moreover, the beams also performed according to the expected structural behaviour where the first crack initiated directly under or close to the loading point, yet all the beams exhibited an identical failure mechanism where an inclined crack would suddenly propagate along the reinforcement causing an abrupt and complete loss of the load bearing capacity (see Figure 3). The agreement of the structural results among the different beam specimens is indicative of a good level of uniformity of the concrete properties and reinforcement position, which is very favourable to test the repeatability of the DOFS for the purpose of crack monitoring.

In the following sections, the results of investigating different aspects related to the ability of DOFS to provide meaningful quantitative information about the cracking process of RC elements are presented and discussed. Firstly, the accuracy of the strain measurements provided by the optical fiber sensors are tested against the local measurements of electrical foil gauges. Subsequently, the suitability of DOFS to fulfil the different levels of a SHM system, namely detection, location and quantification of crack damage, are addressed.

3.1. Correlation between DOFS and strain gauges

The evolution of the strain measurements obtained by the foil strain gauge over the duration of the tests is presented in Figure 4 together with the corresponding strain measured by the optical fiber at the mid-span for all the beam specimens tested.

As observed, an excellent agreement between the optical fiber and the foil gauge was generally obtained regarding both the shape and the value of the strain profiles. Beam 3 and beam 5 presented small discrepancies between both sensors at the end and beginning of the test, respectively. Several factors may have contributed to such discrepancies, the most obvious being the fact that each sensor was attached to a different reinforcement bar of the same beam, causing that cracks propagating in an arbitrary direction which is not completely straight nor perpendicular to the reinforcement might have crossed the rebars at different locations. Other possible reasons for the discrepancies found for beams 3 and 5 could be the removal of a rib in one of the bars to accommodate the foil gauge or even a difference in the relative position of the foil gauge and the DOFS on the rebar, as local bending of the bar has been shown to yield a noticeable variation in the strain measurements (Davis et al., 2017). As a result, an actual difference in strains between the mid-span of each rebar may be expected.

Moreover, during the execution of the loading test for beam 6, the misplacement of the hinge between the jack and the beam caused a loss of contact due to excessive rotation that resulted in the complete unloading of the beam. This is apparent in Figure 4 by a plateau in the strain curves of beam 6 of approximately 5 min. It is noteworthy that even after the complete unloading of the beam, both sensors displayed a consistent behaviour revealing a significant amount of inelastic strain at the reinforcement. Those results confirm that bonding an optical fiber sensor directly onto the reinforcement with cyanoacrylate adhesive and protected by a layer of silicone can provide results as accurate as those provided by conventional foil strain gauges, without the need of altering the reinforcement by either grinding down ribs or edging a groove.

Table 3. Summary of structural performance results of the three-point bending tests.

Specimen	Loading type	Max. load [kN]	Max. deflection [mm]	Number of cracks
Beam 1	Monotonic	39.11	2.27	6
Beam 2	Monotonic	40.90	2.34	6
Beam 3	Cyclic	40.52	2.33	7
Beam 4	Cyclic	37.45	1.98	6
Beam 5	Cyclic	38.91	2.11	7
Beam 6	Cyclic	41.04	2.17	7

3.2. Damage detection: formation of the first flexural crack

The most basic level of a SHM system, sometimes referred to as anomaly detection, is the detection of damage, which is often based on the identification of states that deviate significantly from what is considered a normal state. Cracking of concrete cannot be strictly considered an anomaly since cracking is an inherent process to the structural behaviour of reinforced concrete structures. Nevertheless, excessively large cracks are regarded as a potential source of durability problems and cracks, in general, induce changes in the

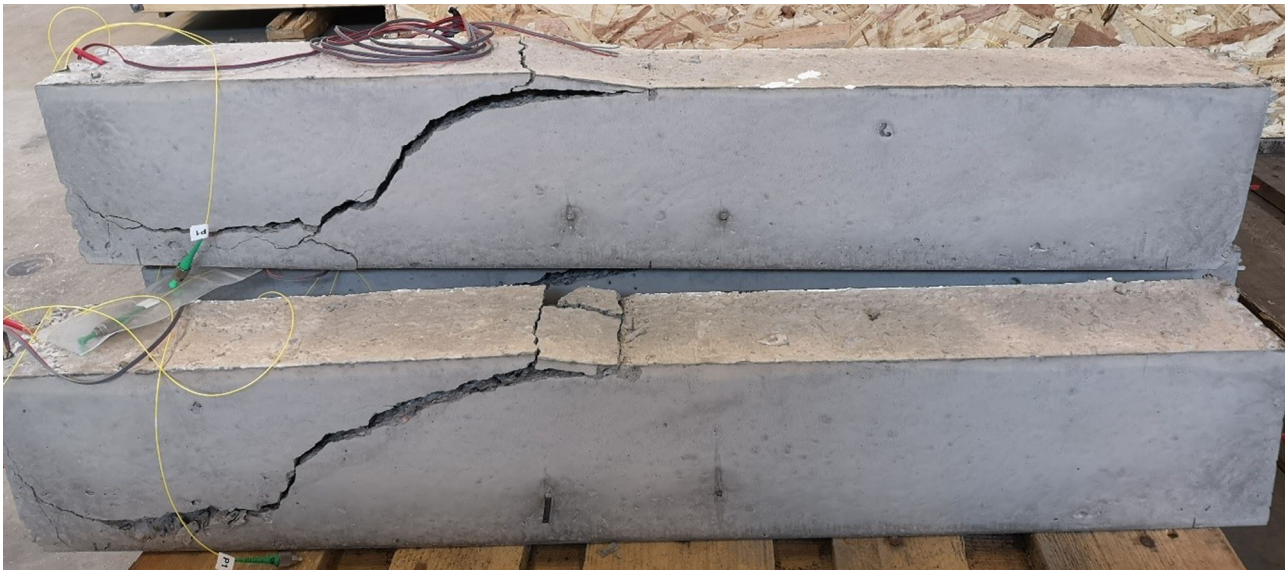

Figure 3. Beam specimens after testing displaying the developed shear failure mechanism.

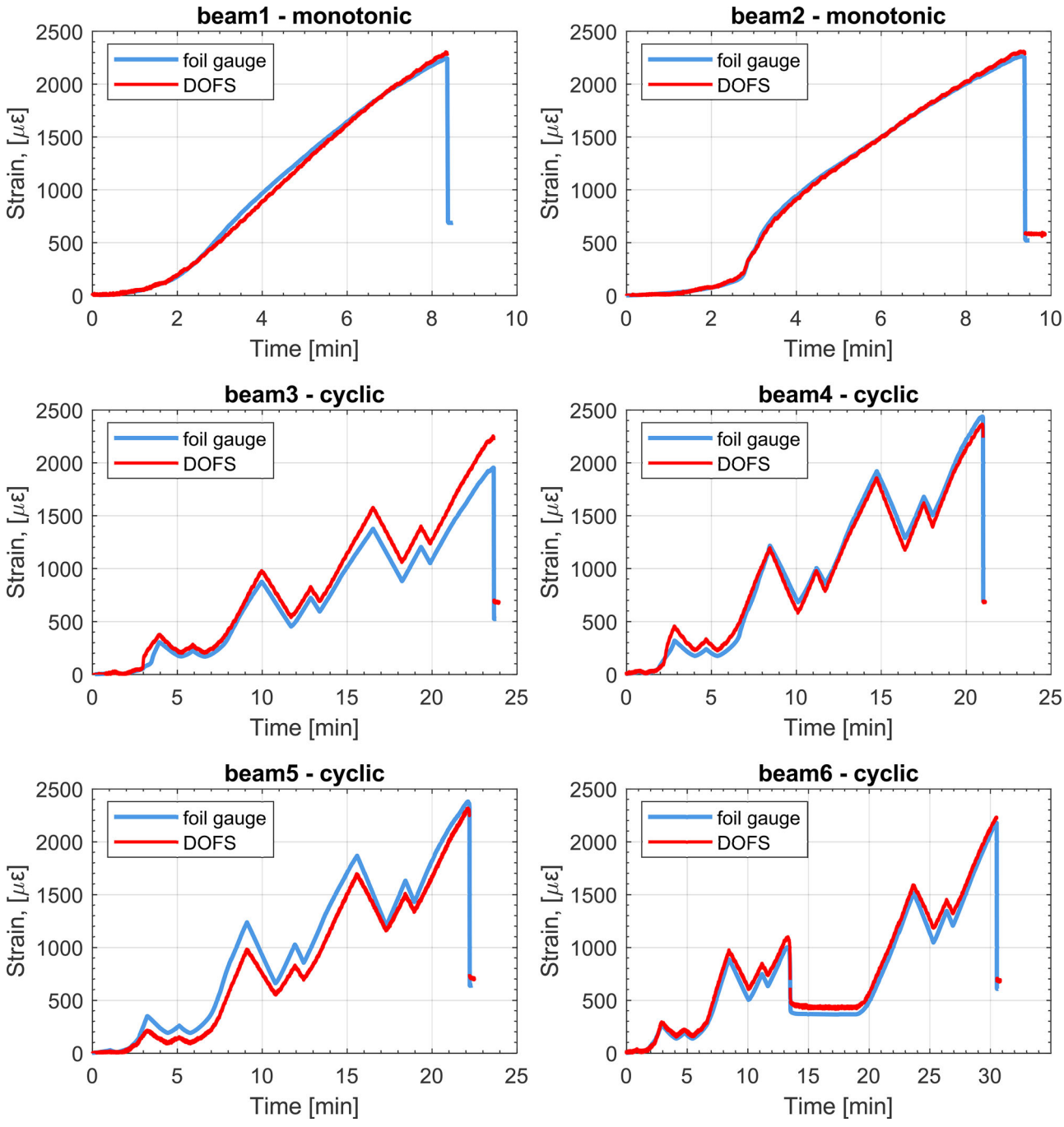

Figure 4. Time evolution of the reinforcement strain during the three-point loading tests measured by the electrical foil gauges and DOFS for all the tested beam specimens.

structure that clearly differentiate the uncracked and cracked states.

In the cracks, the contribution of the concrete to the transfer of tensile stresses is negligible. As a result, the moment of inertia of the cracked sections is greatly reduced, thus leading to increased local strain in the reinforcement and greater curvature of the section, which in turn reduces the bending stiffness of the structure. Whereas the detection of cracks is straight forward when the fiber sensor is bonded to the surface of the concrete due to appearance of large strain discontinuities, the strain gradient in the reinforcement is less apparent. One way to determine the onset of cracking is by finding deviations between the measured strain profiles and the theoretical ones given by classical beam theory assuming elastic behaviour of the materials and perfect bond between the concrete and the reinforcement, see e.g. (Carrera, Giunta, & Petrolo, 2011). The corresponding longitudinal strain at the reinforcement for each position $\varepsilon(x)$, in the uncracked state, can be calculated according to:

$$\varepsilon(x) = \frac{M_y(x)}{E_c I_y^*} z \tag{1}$$

where $M_y(x)$ is the in-plane bending moment, z is the distance to the neutral axis of the transformed section and E_c is the modulus of elasticity of the concrete, which is taken

as 35 GPa, and was obtained from the formulation proposed in the Eurocode 2 (EN 1992-1-1 Eurocode 2, 2, 2004) using the value of the mean cube compressive strength included in Table 2. I_y^* is the moment of inertia of the transformed concrete section defined as:

$$I_y^* = I_c + A_c d_c^2 + (\alpha - 1) A_s d_s^2 \quad (2)$$

where I_c is the moment of inertia of the brut concrete section, A_c is the concrete brut area, A_s is the reinforcement area, α is the modular ratio of steel to concrete E_s/E_c and d_c and d_s are the distance between the neutral axis of the transformed section and the centroids of the concrete brut section and reinforcement respectively.

In Figure 5, a comparison between the theoretical and measured strain profiles along the length of the beam is presented for all the beams at two different load levels, namely for a point load of $P = 2$ kN and for the cracking load, P_{cr}. Owing to the small strain levels attained at the reinforcement before the formation of cracks and the signal noise of the optical fiber sensors which ranged between ±10 με, the noise to signal ratio of the DOFS measurements made it difficult to have a clear comparison. It should be noted that the signal noise in this study was similar to that reported by Barrias, Casas, and Villalba (2019b) but significantly higher than that obtained by others, see e.g. (Henault et al., 2012) who reported values as small as 2 με. This increased signal noise might be attributed to the settings of the analyser, namely the small gauge length and high sampling frequency, and could have been potentially mitigated by choosing a larger gauge length. Nevertheless, as suggested by Barrias et al. (2019b), a filtering operation consisting on a moving average over a length of 10 mm was performed to remove part of the noise.

As observed in Figure 5, a fair agreement exists between the theoretical and the measured strain profiles for the lower load level, despite the latter being still somewhat noisy after filtering. Conversely, the theoretical and measured strain profiles are visibly different at the cracking load, where the latter presents apparent strain localization near the mid-span. It should be highlighted that at the load level of the cracking load, i.e. about 5 kN, the measured crack width was approximately 40 μm as measured by the DIC, hence imperceptible to the naked eye. However, in this study the detection of cracks below that value based on the strain profiles obtained by the DOFS bonded to the reinforcement was not obvious, whereas a DOFS bonded to the concrete surface could have clearly detected cracks as small as 10 μm, see e.g. (Brault & Hoult, 2019b). Nevertheless, the method used in this study might perform better in cases where the expected strain profile is constant, such as uniform bending moment regions or member in tension, since the concentration of strain would be more easily discernible.

3.3. Determination of crack position

As previously mentioned, one of the main advantages of DOFS based on OFDR of Rayleigh scattering is the unprecedented spatial resolution achieved, reaching the submillimetre scale. It is precisely that spatial resolution what enables the obtention of truly distributed strain profiles along the reinforcement which can be analysed to detect variations that may be associated to the existence of cracks in the concrete.

The procedure used to compare the crack position obtained from the DIC measurements and the crack position as determined from the strain profiles measured with the DOFS is presented in Figure 6. As observed, the cracks formed at the surface of the concrete are clearly distinguishable from the 2 D strain field plot provided by the DIC. Note, however, that the image is noisy towards the edges of the beam where some strain information is even lost at specific regions. This was attributed to the images being slightly out of focus in those regions, thus leading to the inability of the software to accurately track the displacement of image subsets.

Consequently, the large strain values that can be randomly spotted near the edges were ignored in the outermost 100 mm of each end. Moreover, since cracks were generally somewhat inclined or discontinuous (see mid-span crack in Figure 6(a), in order to automatically extract the crack position from DIC results in a consistent way, the following procedure was implemented: (i) three longitudinal profiles of the surface strain at the level of the reinforcement and at ± ∅/2 were obtained; (ii) for each longitudinal profile, an initial thresholding was applied to remove all the peaks with a strain lower than 1% (i.e. to remove noise and cracks with a width smaller than approximately 50 μm); (iii) each profile was then transformed by fitting a gaussian distribution with maximum height of 1 and standard deviation of 7 to every peak remaining after the thresholding and adding them together; (iv) the harmonic mean of the three transformed profiles was performed to obtain the profile use to determine the position of the cracks, which is illustrated in Figure 6(b) as a black line. It should be noted that only fully formed active cracks were tracked, i.e. red regions in Figure 6(a), whereas incipient and closing cracks which displayed low strain values in the DIC results were not considered in the comparison.

In Figure 6(c), a series of curves show the evolution of the strain profiles measured by the DOFS during the cyclic loading test of beam 4. Following the same rationale introduced in the previous section, cracks can be associated to local peaks in the strain profile of the reinforcement. Away from the crack, the strain at the reinforcement decreases as the load is partially transferred to the concrete due to bond action until compatibility of strains is reached or until the concrete reaches its tensile strength, where a new crack would form. However, for a new crack to form, a certain length is required to build up sufficient stress in the concrete, noted as the minimum transmission length, $l_{t,min}$. As a result, new cracks can continue forming until the separation between them is no greater than the minimum crack spacing $s_{r,min} = 2 \cdot l_{t,min}$. The crack spacing can generally range from just a few centimetres to several tens of centimetres depending on the bond properties between the

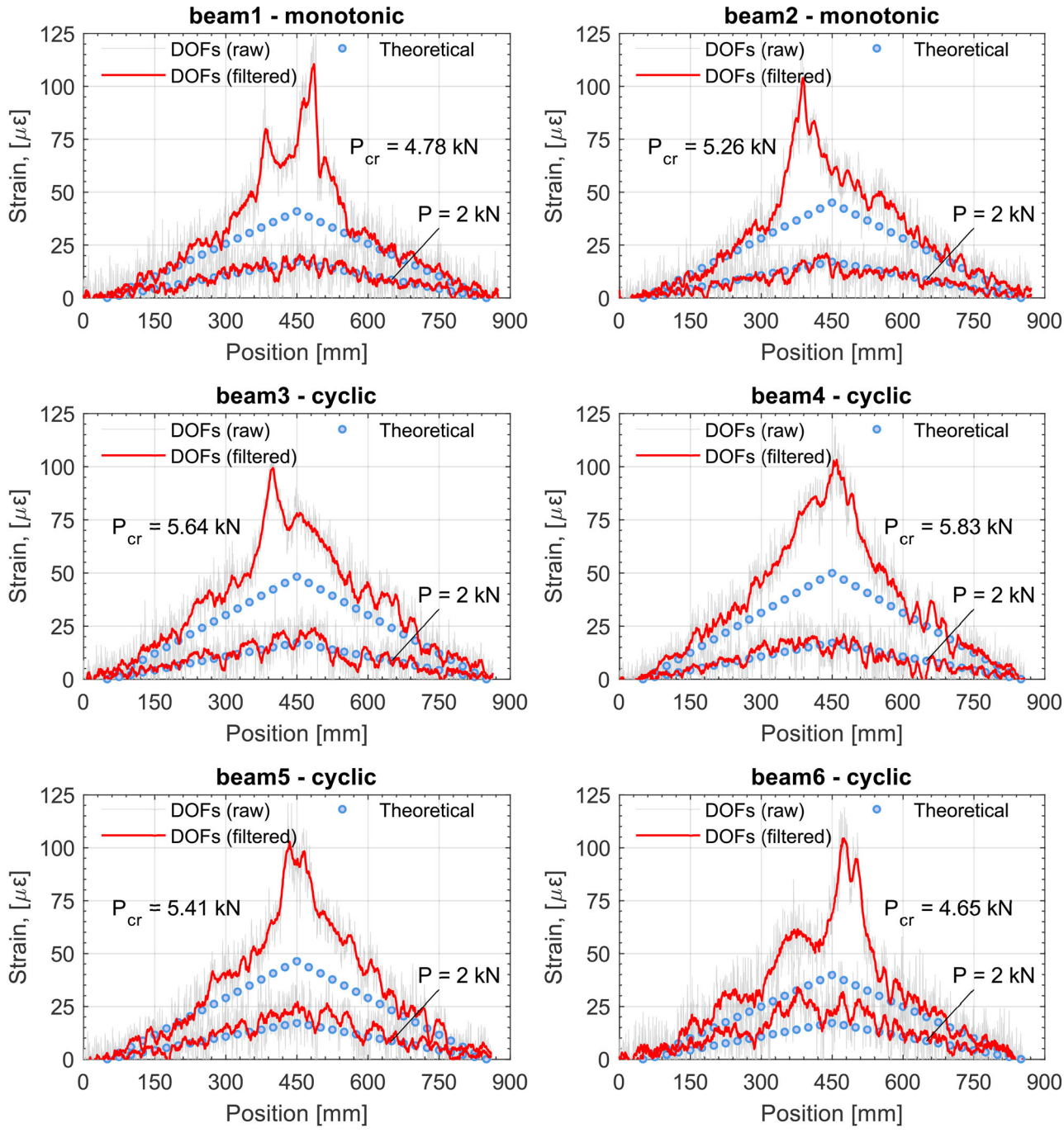

Figure 5. Comparison of theoretical and measured strain profiles obtained with the DOFS along the beam length for a load level of 2 kN and at the cracking load, Pcr. A moving average filter over a 10 mm length is applied to the measured strain profiles to decrease the noise to signal ratio.

concrete and the reinforcement, the reinforcement ratio and the rebar diameter.

Consequently, using the above requirement as a basis to discriminate the peaks associated to cracks in the strain profile, a smoothing spline was fit to the strain profile corresponding to the maximum load, where a stabilized crack pattern had already been reached, to get rid of all the peaks associated to the spatial resolution noise. Subsequently, the derivative of the fit curve was analysed to select only those peaks where the sum of the absolute value of the maximum gradient before and after the peak was equal or larger than 10 με/mm. This threshold was found suitable to discern between fully formed cracks, as detected by the DIC, and other potential types of crack or defects, such as secondary internal cracks that might not be visible at the surface (Goto, 1971). Finally, the position of the cracks determined by the optical fiber are represented by the red triangular markers in Figure 6(c), whereas the grey shaded areas correspond to the crack positions determined from the DIC.

Figure 7 illustrates the accuracy of the DOFS to locate the position of cracks taking the measurements of the DIC as the correct crack position. Figure 7(a), shows, qualitatively, that a fair agreement is attained between the results of the optical fiber and the DIC, whereas Figure 7(b) displays the error difference between both measurements, $e = x_{DIC} - x_{DOFS}$, as a function of the crack position. As

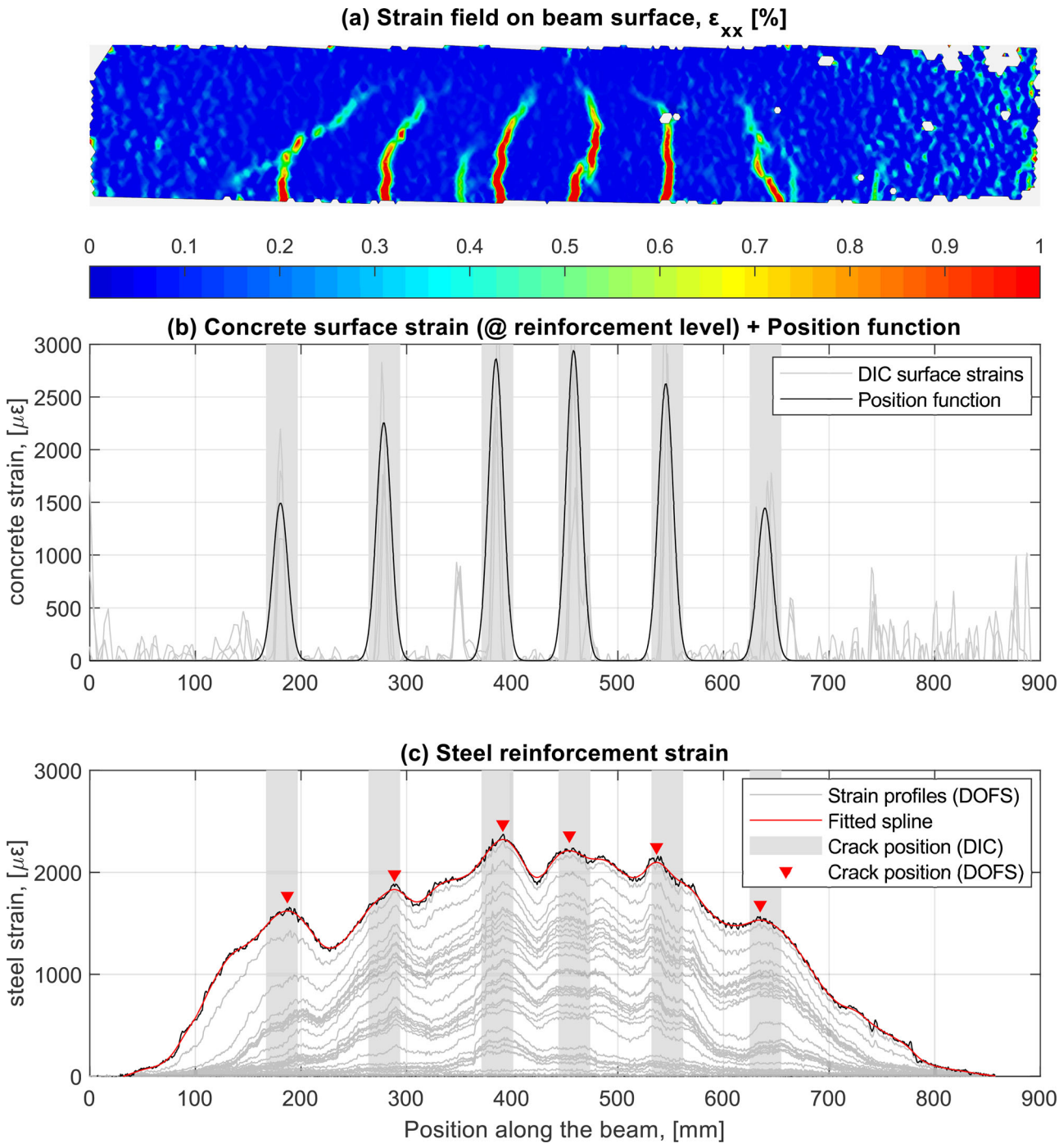

Figure 6. Example of the procedure used to obtain and compare the crack location from DIC and DOFS for beam 4: (a) two dimensional strain field on the concrete surface from DIC; (b) combined profiles of the concrete surface strain at the level of the reinforcement from the DIC, where the position of the cracks has been highlighted by grey shaded areas; (c) multiple strain profiles from the DOFS where the red triangular makers indicate the determined crack position based on the strain profile at maximum load and the grey shaded area correspond to position determined from the DIC.

observed, all the errors were within the range ±30 mm with the exception of three cracks whose position was mispredicted by almost 50 mm. It should be noted, however, that these results compare measurements of the same cracks at the surface and the reinforcement level. Since those cracks might not propagate perfectly perpendicular to the longitudinal axis of the beam, part of the observed error could be potentially attributed to an actual difference between the position of the cracks at different depths. Moreover, it is interesting to note that the amount of positive and negative errors is rather evenly distributed but a slight tendency is apparent where the crack position was underestimated by the DOFS at low x coordinates and, conversely, it was overestimated at high coordinate x coordinates.

A potential explanation for this behaviour could be attributed to the existence of secondary inclined cracks growing from the cracks closer to the supports, which may induce a small shift in the position of the strain peak, as for the crack near the coordinate $x = 200$ mm in Figure 6(c). This is in line with the findings by (Brault & Hoult, 2019a)

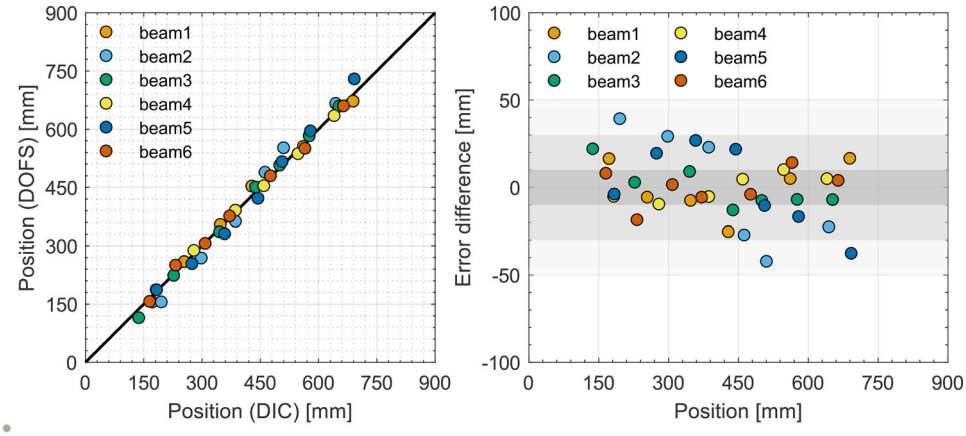

Figure 7. Comparison of the crack position determined by the DOFS and the DIC system (left) and quantitative error difference between both measurements for every crack of all the beams tested (right).

who observed that the strain in the reinforcement crossing cracks with predominant in-plane shear stresses displaying loading mode-II deviated from strains predicted by beam theory.

3.4. Crack width evaluation based on reinforcement strain DOFS measurements

The last aspect investigated in the present study is the feasibility of using DOFS strain measurements to provide quantitative information regarding the crack width of existing cracks. As briefly discussed in Section 1, for coated optical fiber sensors bonded directly onto the concrete, Feng et al. (Feng et al., 2013) proposed a mechanical model based on shear lag theory to relate the crack opening displacement to the strain in the fibre core. However, one of the assumptions in that model is the perfect bond between all the intermediate layers. Since the opening of cracks is the result of the relative displacement between concrete and the reinforcement, that model is, in principle, not applicable to optical fiber sensors bonded to the reinforcement.

Referring to current structural design codes, e.g. Eurocode 2 (EN 1992-1-1 Eurocode 2, 2, 2004), the calculation of the crack width in reinforced concrete structures is based on mechanical models derived from the study of thin members subjected to direct tension. Those models state that the characteristic crack width, w_k, can be calculated as:

$$w_k = s_{r,max}\ (\varepsilon_{sm} - \varepsilon_{cm}) \tag{3}$$

where $s_{r,max}$ is the maximum crack spacing and ε_{sm} and ε_{cm} are the mean strain at the steel and concrete, respectively. In such models, the parameters in Equation (3) are obtained from the equilibrium of tensile forces between the crack section and a section located at $0.5{\cdot}s_{r,max}$ from the previous one when the stress in the concrete reaches its tensile capacity, f_{ct}. The expressions used, however, often involve several empirical parameters to characterize the bond behaviour between steel and concrete, the type of reinforcement, the duration of the load, etc., which are the factors governing the variation of strain along the reinforcement.

In the present investigation, a similar approach to that included in structural design codes, expressed by Equation (3), and used by other researchers for DOFS bonded to the concrete surface (cf. Brault & Hoult, 2019b), was adopted with appropriate modifications. The proposed method assumes that the variation of the strain along the reinforcement is known and that the position of the cracks, and therefore the crack spacing, can be obtained from the DOFS measurements following the procedure described in the previous section. Furthermore, it is assumed that in the absence of interaction between the reinforcement and the surrounding concrete, the variation of stress and strain in the reinforcement should follow the moment distribution, namely a linear variation for three-point loading. Consequently, it can be inferred that the non-linear variation of strain between cracks measured by the DOFS must include the effect of the stress transfer between the reinforcement and the concrete due to bond action. Accordingly, the following expression is suggested to calculate the crack width:

$$w_{cr,i} = \int_{-l_{t,i}^{-}}^{l_{t,i}^{+}} \varepsilon^{DOFS}(x)\ dx - \rho\alpha \left[\int_{-l_{t,i}}^{l_{t,i}^{+}} \hat{\varepsilon}(x) - \varepsilon^{DOFS}(x) dx \right] \tag{4}$$

where $\varepsilon^{DOFS}(x)$ is the strain along the reinforcement measured by the DOFS, $\hat{\varepsilon}(x)$ is the assumed linear strain variation between cracks neglecting the steel-concrete interaction, $\rho = A_s/A_{c,ef}$ and $\alpha = E_s/E_c$ are the reinforcement ratio and the modular ratio, respectively and $l_{t,i}^{-}$ and $l_{t,i}^{+}$ are the transmission length to the left and right sides of the i-th crack, $w_{cr,i}$, along the beam. The proposed method to evaluate crack widths based on DOFS measurements is graphically illustrated in Figure 8, where the two integrals in Equation (4) are represented by the shaded areas in the zoomed region.

It should be noted that, although the position of the cracks is known, the actual boundaries of the integral given by Equation (4) are not clearly defined. In a member with varying moment, the local minima in the strain profile only indicate the points where the rate of change of the strain in the reinforcement due to bond is larger than that due to the moment variation. Nevertheless, the valleys in the strain profile between cracks were taken as a first approximation for the limits of the transmission length, which for the case

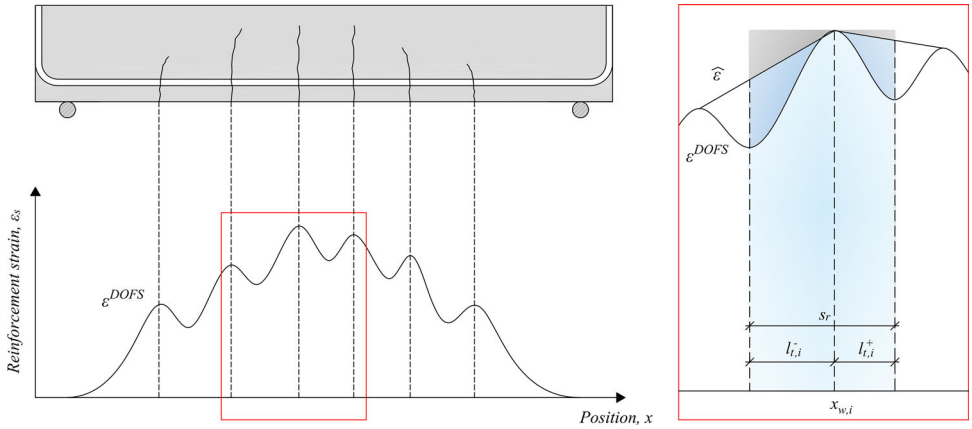

Figure 8. Graphical representation of the method used to estimate the crack width. The integrals in Equation (4) correspond to the shaded areas in the zoom region, where the light blue area represents the contribution of the reinforcement and the dark blue area represents the contribution of the concrete between cracks.

of constant bending moment and pure tension state would be an accurate choice.

Based on the described method, the crack widths of each individual crack in every beam were calculated for all the load steps. Figure 9 shows a comparison of the calculated crack width and the crack width measurements from the DIC for the widest crack of each beam. It can be observed that, in general, the crack width estimation of the widest crack based on the DOFS correlated well with the DIC measurements, even for the cyclically loaded beams, where the predicted crack widths followed the closing and re-opening of cracks upon unloading and reloading.

However, it can be also seen that for beams 1 and 3, the crack width estimated by the DOFS started overestimating the DIC measurements for crack widths larger than 0.2 mm. As discussed by (Brault & Hoult, 2019b), this could be attributed to a reduction of the DOFS accuracy for large strain where more anomalous readings may be present in the strain profile. The crack width of Beam 6 agreed well with the DIC measurements up to the point where the loading was accidentally halted. Thereafter, the calculated crack width consistently underestimated the DIC crack width. Even though the DOFS and DIC measurements were not interrupted, a slight misplacement of the loading plate might have caused a subtle change in the load position and consequently a change in the moment and strain distribution.

Furthermore, the calculated crack width for beam 2 displayed a weak correlation with DIC crack width measurements. Considering that beam 2 exhibited the largest difference between the predicted crack location and the measured by DIC, as shown in Figure 7, one possible explanation for the weak performance of the proposed method could be the low accuracy in the determination of the crack locations, which subsequently might have led to erroneous crack width calculations.

In Figure 10, the distribution of crack width errors, $e = w_{cr}^{DOFS} - w_{cr}^{DIC}$, for each individual crack in every beam is presented. Figure 10 reveals several interesting aspects of the proposed crack width measurement technique. The first is that, except for beam 2, the crack width errors seem to be symmetrically distributed around zero, i.e. some cracks are overestimated while other are underestimated. Small underestimations could be explained by the fact that the crack width calculated is at the reinforcement level whereas the crack width measured by DIC is at the surface, which may be potentially larger. However, for a concrete cover of only 25 mm as in this study, this effect was most likely very small. Crack width overestimations, on the other hand, could be attributed to the existence of incipient or internal cracks forming in the vicinity of fully formed cracks, which were not considered in this work. Another interesting aspect is that, unlike what it was anticipated, the combination of mode-I and mode-II loading for cracks formed in predominantly shear loaded regions did not seem to affect negatively the accuracy of the proposed method, i.e. cracks closest to the supports did not show larger errors compared to other cracks.

It is also interesting to note that the largest crack width errors were concentrated in half of the beams, namely beam 2, 5 and 6, whereas beams 1, 3 and 4 showed systematically better correlations with the DIC measurements. However, the crack width errors did not seem to be correlated with the crack location errors. A simple explanation for this observation is that, in fact, the most relevant points are the "valleys", which define the integration limits. As long as the position of the cracks are determined to be between the two adjacent valleys, the actual position of the crack will not affect the first integral in Equation (4), which is the main contribution to the crack width. In the light of these results, the larger crack width error in some of the beams can be indicative that the accuracy of the DOFS measurements was lower for some of the tests, suggesting the appearance of anomalous readings.

It should be highlighted that, even though the accuracy of the proposed method could be potentially improved by increasing the quality of the DOFS measurements (adjusting the analyser settings to use longer gauge length or using other types of fiber sensors, such as nylon-coated fibers), in most cases, the calculated crack widths differed in less than 20 μm with the crack width measurements from the DIC, which for crack widths between 0.1 and 0.2 mm represent an error of less than 20%. This error in crack width may be

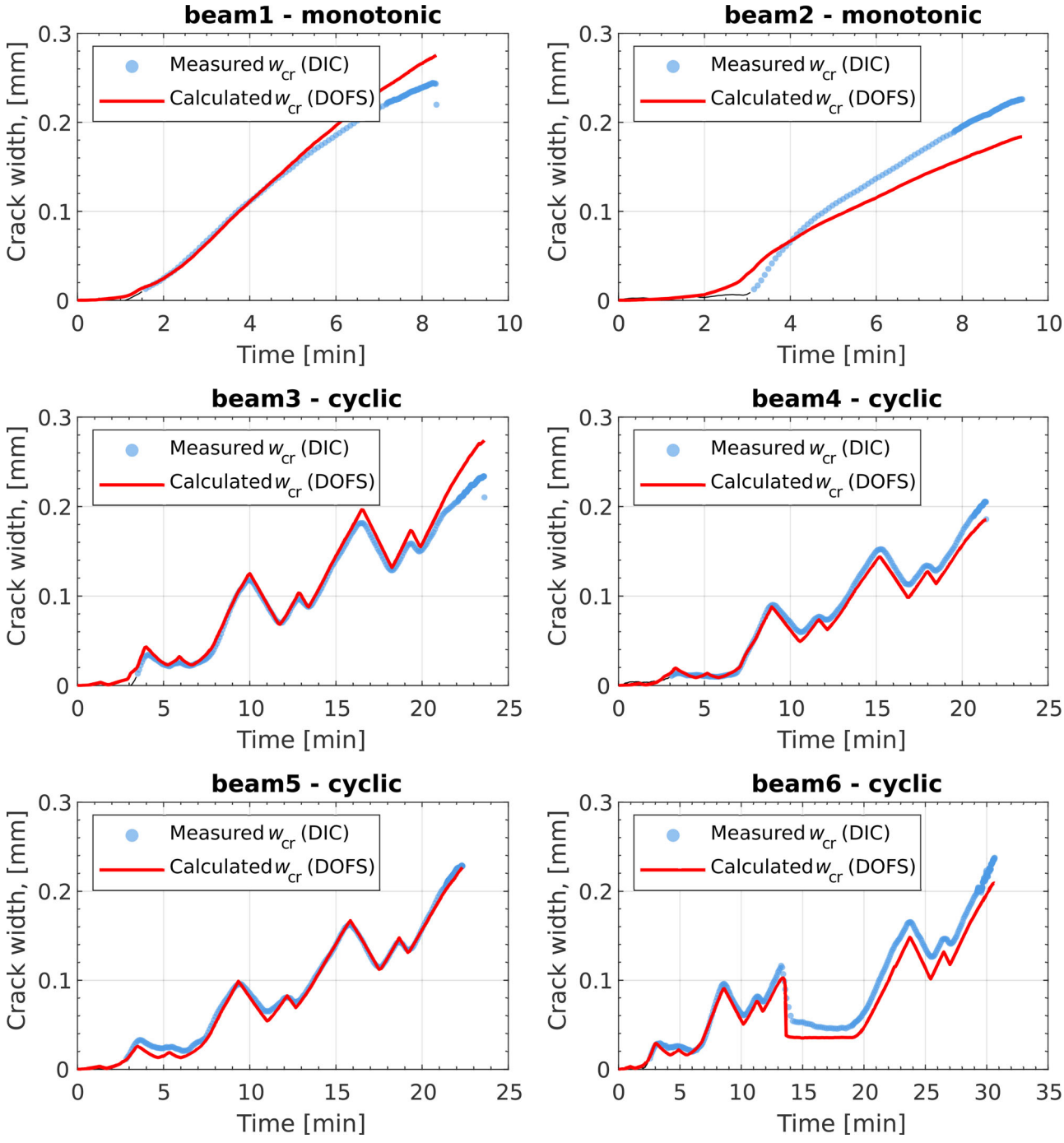

Figure 9. Comparison between the crack width measured by the DIC and calculated from the DOFS measurements based on the Equation (4), for the widest crack in each beam specimen.

considered as acceptable in the absence of more accurate measurements. Particularly, it offers obvious advantages with respect to other techniques as it provides an estimation of the crack width for each individual crack detected by the optical fiber sensor. Moreover, unlike for displacement transducers, the location of cracks is not needed in advanced, which means that the proposed method based on DOFS can be used to measure the entire crack width history. Nevertheless, remaining questions to be explored are related to the ability of DOFS to maintain the same level of accuracy under long-term loading or in structures subjected to expansive deterioration mechanisms that might affect the strain at the reinforcement such as corrosion, sulphate attack or alkali-silica reaction.

4. Conclusions

This paper explored the viability of using a relatively recent technology, namely distributed optical fiber sensors (DOFS) based on Optical Frequency Domain Reflectometry (OFDR) of Rayleigh backscattering, for crack monitoring purposes in concrete structures. Through a series of laboratory experiments consisting of three-point bending tests of reinforced

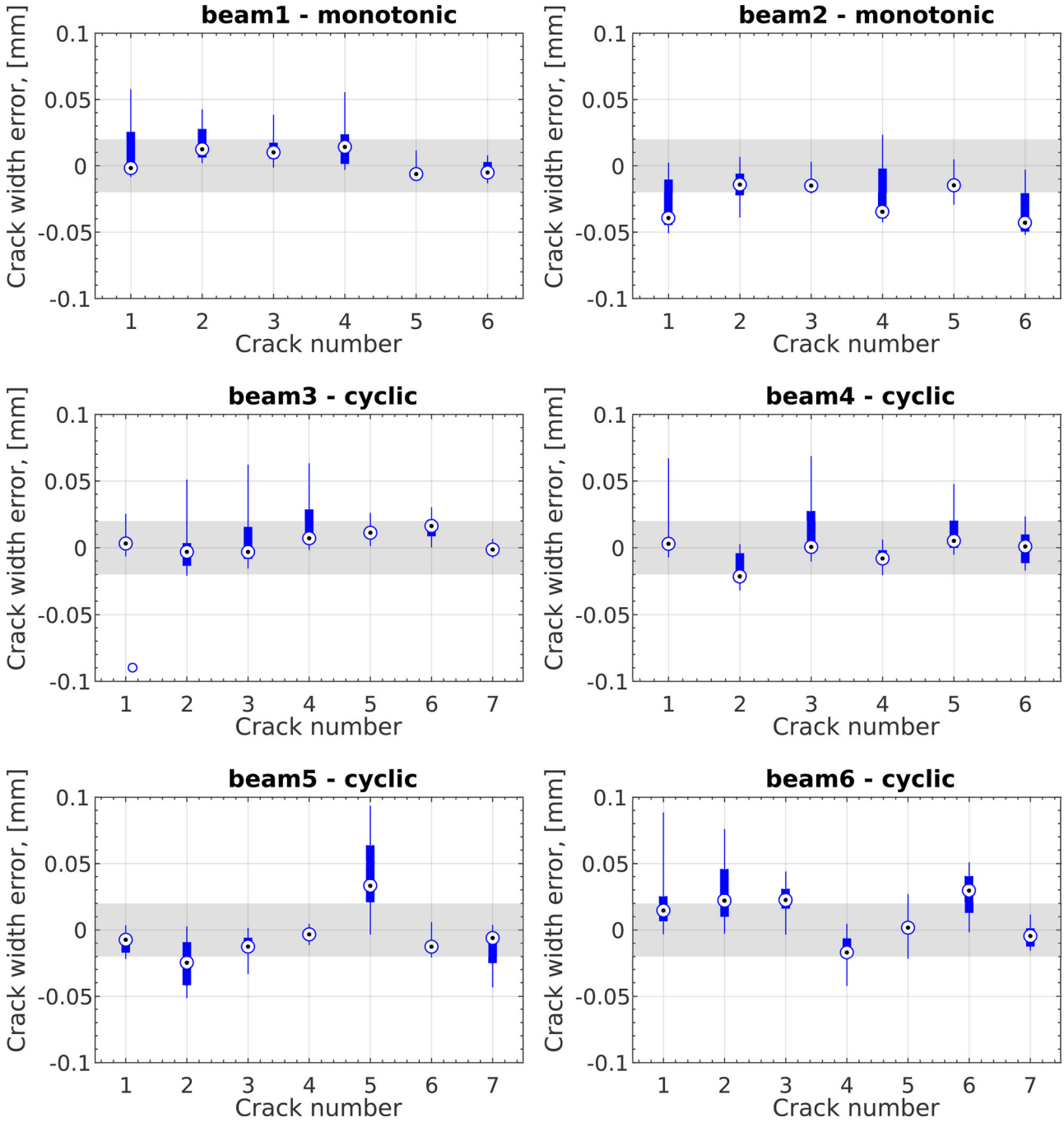

Figure 10. Error difference between the calculated crack width based DOFS measurements and the crack width measured by the DIC for each crack in each of the tested beam specimens. Central markers indicate median values, the boxes indicate the 25th and 75th percentiles and the whiskers indicate the extreme data values not considered as outliers. Outliers are indicated by peripherical individual markers.

concrete beams, the authors investigated the suitability of using DOFS to provide meaningful information about the formation, location and quantification of crack width. Moreover, in the present work the DOFS were deployed directly onto the reinforcement using a protective layer of silicone, without any previous mechanical modification of the reinforcement to accommodate the optical fibers. Electrical foil gauges and Digital Image Correlation were used to validate the DOFS measurements on monotonic and cyclic loading tests.

Overall, the DOFS system provided strain measurements that agreed well with those measured by conventional electrical foil gauges throughout the entire test up to the failure of the beams, both for monotonic and cyclic tests. Even though the noise to signal ratio of the DOFS measurements was high within the elastic range of the bending tests, the strains measured experimentally correlated well with those calculated based on traditional beam theory. Moreover, excellent repeatability was obtained among the six beams tested.

Unlike traditional strain gauges and other quasi-distributed optical fiber sensing systems which offer discrete measurements with a gauge pitch that can be down to a few centimetres, the system used in the present study delivered an unprecedented spatial resolution of only 0.65 mm. Nevertheless, the use of such a small gauge length led to

significant spatial variability of the measurements, especially at low strains. The application of an averaging filter over a 1 cm region to the DOFS strain measurements was beneficial to visualise and compare the results.

The fiber sensor deployment methodology tested enabled the successful detection of crack formation at an early stage, i.e. for cracks as small as 40 µm. Even though at that level cracks are still not perceptible to the human eye, a fiber sensor bonded to the concrete surface or embedded in the concrete would provided even earlier detection capabilities. However, bonding the fiber to the reinforcement can reduce the risk of fiber rupture, as well as idle readings caused by exceeding the strain range of the sensor, since no strain discontinuities occur in the reinforcement.

It was found that based on the strain distribution at the reinforcement provided by the DOFS, it is feasible to locate the position of active fully-formed cracks which can be associated to local peaks of strain. However, the determination of the crack position is less apparent than for sensors bonded to the surface or embedded in the concrete and it required a certain post-processing of the strain data to remove the noise associated to the spatial variability. Nevertheless, the comparison of the crack location obtained from the DIC and from the DOFS measurements revealed that most cracks were located within an acceptable range of ±3 cm. Considering that cracks are measured at different depths, i.e. at the surface and at the reinforcement level, and that the crack planes might not be perfectly perpendicular to the direction of the reinforcement, that difference might not be entirely attributable to an error of the crack location based on the DOFS measurements.

Lastly, the capabilities of the DOFS to provide quantitative information about the crack width were demonstrated. By integrating the strain profile over a certain length adjacent to the crack and removing the contribution of the tension stiffening between cracks, good agreement was generally achieved with the DIC results, being the error for most estimated crack widths within ±20 µm. While the proposed method to estimate crack widths was not found to be very sensitive to the exactness of the crack positions, a higher quality of DOFS strain measurements could potentially increase the accuracy of the method, thereby reducing the crack width errors for cracks beyond 0.2 mm.

Disclosure statement

No potential conflict of interest was reported by the author(s).

Funding

This work was supported by the Swedish Transport Administration (Trafikverket) under the grant TRV/BBT 2017-028.

ORCID

Carlos G. Berrocal http://orcid.org/0000-0003-4654-5498
Ignasi Fernandez http://orcid.org/0000-0003-4847-2894
Rasmus Rempling http://orcid.org/0000-0002-1122-7855

References

Bado, M., Casas, J., & Barrias, A. (2018). Performance of Rayleigh-based distributed optical fiber sensors bonded to reinforcing bars in bending. *Sensors*, *18*(9), 3125. doi:10.3390/s18093125

Bao, Y., & Chen, G. (2015). Strain distribution and crack detection in thin unbonded concrete pavement overlays with fully distributed fiber optic sensors. *Optical Engineering*, *55*(1), 11008. doi:10.1117/1.OE.55.1.011008

Bao, Y., Meng, W., Chen, Y., Chen, G., & Khayat, K. H. (2015). Measuring mortar shrinkage and cracking by pulse pre-pump Brillouin optical time domain analysis with a single optical fiber. *Materials Letters*, *145*, 344–346. doi:10.1016/j.matlet.2015.01.140

Barrias, A., Casas, J. R., & Villalba, S. (2016). A review of distributed optical fiber sensors for civil engineering applications. *Sensors*, *16*(5), 748. doi:10.3390/s16050748

Barrias, A., Casas, J. R., & Villalba, S. (2017). Application study of embedded Rayleigh based distributed optical fiber sensors in concrete beams. *Procedia Engineering*, *199*(2017), 2014–2019. doi:10.1016/j.proeng.2017.09.466

Barrias, A., Casas, J. R., & Villalba, S. (2019a). Distributed optical fibre sensors in concrete structures: Performance of bonding adhesives and influence of spatial resolution. *Structural Control and Health Monitoring*, *26*(3), e2310. doi:10.1002/stc.2310

Barrias, A., Casas, J. R., & Villalba, S. (2019b). SHM of reinforced concrete elements by Rayleigh backscattering DOFS. *Frontiers in Built Environment*, *5*(March), 1–14. doi:10.3389/fbuil.2019.00030

Barrias, A., Casas, J., & Villalba, S. (2018). Embedded distributed optical fiber sensors in reinforced concrete structures—A case study. *Sensors*, *18*(4), 980. doi:10.3390/s18040980

Barrias, A., Rodriguez, G., Casas, J. R., & Villalba, S. (2018). Application of distributed optical fiber sensors for the health monitoring of two real structures in Barcelona. *Structure and Infrastructure Engineering*, *14*(7), 967–985. doi:10.1080/15732479.2018.1438479

Bassil, A., Wang, X., Chapeleau, X., Niederleithinger, E., Abraham, O., & Leduc, D. (2019). Distributed fiber optics sensing and coda wave interferometry techniques for damage monitoring in concrete structures. *Sensors*, *19*(2), 356. doi:10.3390/s19020356

Billon, A., Hénault, J.-M., Quiertant, M., Taillade, F., Khadour, A., Martin, R.-P., & Benzarti, K. (2015). Qualification of a distributed optical fiber sensor bonded to the surface of a concrete structure: a methodology to obtain quantitative strain measurements. *Smart Materials and Structures*, *24*(11), 115001. doi:10.1088/0964-1726/24/11/115001

Brault, A., & Hoult, N. (2019a). Distributed reinforcement strains: Measurement and application. *ACI Structural Journal*, *116*(4), 115–127. doi:10.14359/51714483

Brault, A., & Hoult, N. (2019b). Monitoring reinforced concrete serviceability performance using fiber-optic sensors. *ACI Structural Journal*, *116*(1), 57–70. doi:10.14359/51710870

Brault, A., Hoult, N. A., Greenough, T., & Trudeau, I. (2019). Monitoring of beams in an RC building during a load test using distributed sensors. *Journal of Performance of Constructed Facilities*, *33*(1), 4018096. doi:10.1061/(ASCE)CF.1943-5509.0001250

Carrera, E., Giunta, G., & Petrolo, M. (2011). The Euler-Bernoulli and Timoshenko theories. In *Beam structures* (pp. 9–22). NJ, USA: Wiley. doi:10.1002/9781119978565.ch2

Casas, J. R., & Cruz, P. J. S. (2003). Fiber optic sensors for bridge monitoring. *Journal of Bridge Engineering*, *8*(6), 362–373. doi:10.1061/(ASCE)1084-0702(2003)8:6(362)

Cawley, P. (2018). Structural health monitoring: Closing the gap between research and industrial deployment. *Structural Health Monitoring*, *17*(5), 1225–1244. doi:10.1177/1475921717750047

Davis, M. A., Bellemore, D. G., & Kersey, A. D. (1997). Distributed fiber Bragg grating strain sensing in reinforced concrete structural components. *Cement and Concrete Composites*, *19*(1), 45–57. doi:10.1016/S0958-9465(96)00042-X

Davis, M. B., Hoult, N. A., Bajaj, S., & Bentz, E. C. (2017). Distributed sensing for shrinkage and tension stiffening measurement. *ACI Structural Journal*, *114*(3), 753–764. doi:10.14359/51689463

Ding, Z., Wang, C., Liu, K., Jiang, J., Yang, D., Pan, G., … Liu, T. (2018). Distributed optical fiber sensors based on optical frequency domain reflectometry: A review. *Sensors*, *18*(4), 1072. doi:10.3390/s18041072

Du, Y., Chen, Y., Zhuang, Y., Zhu, C., Gerald, R., & Huang, J. (2018). A uniform strain transfer scheme for accurate distributed optical fiber strain measurements in civil structures. *Inventions*, *3*(2), 30. doi:10.3390/inventions3020030

EN 12390-3. (2009). *Testing hardened concrete. Part 3: Compressive strength of test specimens*.

EN 12390-6. (2001). *Testing hardened concrete. Tensile splitting strength of test specimens*.

EN 1992-1-1 Eurocode 2. (2004). *EN 1992-1-1 Eurocode 2: Design of concrete structures—Part 1-1: General rules and rules for buildings*. Brussels, Belgium: CEN.

EN ISO 15630-1. (2019). *Steel for reinforced and prestresed concrete—Testing methods. Part 1: Bars and wires for reinforced concrete*.

Feng, X., Zhou, J., Sun, C., Zhang, X., & Ansari, F. (2013). Theoretical and experimental investigations into crack detection with BOTDR-distributed fiber optic sensors. *Journal of Engineering Mechanics*, *139*(12), 1797–1807. doi:10.1061/(ASCE)EM.1943-7889.0000622

Glišić, B., Hubbell, D., Sigurdardottir, D. H., & Yao, Y. (2013). Damage detection and characterization using long-gauge and distributed fiber optic sensors. *Optical Engineering*, *52*(8), 87101. doi:10.1117/1.OE.52.8.087101

Glišić, B., Posenato, D., & Inaudi, D. (2007). Integrity monitoring of old steel bridge using fiber optic distributed sensors based on Brillouin scattering. In H. F. Wu, A. A. Diaz, & P. J. Shull (Eds.), *Nondestructive characterization for composite materials, aerospace engineering, civil infrastructure, and homeland security 2007* (Vol. 6531, p. 65310P). San Diego, CA: SPIE. doi:10.1117/12.716055

Goto, Y. (1971). Cracks formed in concrete around deformed tension bars. *ACI Journal Proceedings*, *68*(4), 244–251. doi:10.14359/11325

Grzymski, F., Trapko, T., & Musiał, M. (2019). Practical use of distributed fibre optic sensors in research on FRCM composites. In *E3S Web of Conferences* (Vol. 97, p. 2019). France: EDP Sciences. doi:10.1051/e3sconf/20199702019

Güemes, A., Fernández-López, A., & Soller, B. (2010). Optical fiber distributed sensing—Physical principles and applications. *Structural Health Monitoring: An International Journal*, *9*(3), 233–245. doi:10.1177/1475921710365263

Gyger, F., Rochat, E., Chin, S., Niklès, M., & Thévenaz, L. (2014). Extending the sensing range of Brillouin optical time-domain analysis up to 325 km combining four optical repeaters. In J. M. López-Higuera, J. D. C. Jones, M. López-Amo, & J. L. Santos (Eds.), *23rd International Conference on Optical Fibre Sensors* (p. 91576Q). Santander, Spain: SPIE. doi:10.1117/12.2059590

Henault, J.-M., Quiertant, M., Delepine-Lesoille, S., Salin, J., Moreau, G., Taillade, F., & Benzarti, K. (2012). Quantitative strain measurement and crack detection in RC structures using a truly distributed fiber optic sensing system. *Construction and Building Materials*, *37*, 916–923. doi:10.1016/j.conbuildmat.2012.05.029

Imai, M., Nakano, R., Kono, T., Ichinomiya, T., Miura, S., & Mure, M. (2010). Crack detection application for fiber reinforced concrete using BOCDA-based optical fiber strain sensor. *Journal of Structural Engineering*, *136*(8), 1001–1008. doi:10.1061/(ASCE)ST.1943-541X.0000195

Kaklauskas, G., Sokolov, A., Ramanauskas, R., & Jakubovskis, R. (2019). Reinforcement strains in reinforced concrete tensile members recorded by strain gauges and FBG sensors: Experimental and numerical analysis. *Sensors*, *19*(1), 200. doi:10.3390/s19010200

Majumder, M., Gangopadhyay, T. K., Chakraborty, A. K., Dasgupta, K., & Bhattacharya, D. K. (2008). Fibre Bragg gratings in structural health monitoring-Present status and applications. *Sensors and Actuators A: Physical*, *147*(1), 150–164. doi:10.1016/j.sna.2008.04.008

Matta, F., Bastianini, F., Galati, N., Casadei, P., & Nanni, A. (2008). Distributed strain measurement in steel bridge with fiber optic sensors: Validation through diagnostic load test. *Journal of Performance of Constructed Facilities*, *22*(4), 264–273. doi:10.1061/(ASCE)0887-3828(2008)22:4(264)

Morey, W. W., Dunphy, J., & Meltz, G. (1992). Multiplexing fiber Bragg grating sensors. In A. D. Kersey & J. P. Dakin (Eds.), *Distributed and multiplexed fiber optic sensors* (Vol. 1586, pp. 216–224). Boston, MA: SPIE. doi:10.1117/12.56520

Palmieri, L. (2013). Distributed optical fiber sensing based on Rayleigh scattering. *The Open Optics Journal*, *7*(1), 104–127. doi:10.2174/1874328501307010104

Regier, R., & Hoult, N. A. (2015). Concrete deterioration detection using distributed sensors. *Proceedings of the Institution of Civil Engineers—Structures and Buildings*, *168*(2), 118–126. doi:10.1680/stbu.13.00070

Rodriguez, G., Casas, J. R., & Villalba, S. (2015a). Cracking assessment in concrete structures by distributed optical fiber. *Smart Materials and Structures*, *24*(3), 35005. doi:10.1088/0964-1726/24/3/035005

Rodriguez, G., Casas, J. R., & Villalba, S. (2015b). SHM by DOFS in civil engineering: a review. *Structural Monitoring and Maintenance*, *2*(4), 357–382. doi:10.12989/smm.2015.2.4.357

Rodriguez, G., Casas, J. R., & Villalba, S. (2019). Shear crack width assessment in concrete structures by 2D distributed optical fiber. *Engineering Structures*, *195*(May), 508–523. doi:10.1016/j.engstruct.2019.05.079

Seo, J., Hu, J. W., & Lee, J. (2016). Summary review of structural health monitoring applications for highway bridges. *Journal of Performance of Constructed Facilities*, *30*(4), 4015072. doi:10.1061/(ASCE)CF.1943-5509.0000824

Sienko, R., Bednarski, L., & Howiacki, T. (2019). About distributed internal and surface strain measurements within prestressed concrete truck scale platforms. In *IOP Conference Series: Materials Science and Engineering* (Vol. 471, pp. 52074). Bristol, UK: IOP publishing. doi:10.1088/1757-899X/471/5/052074

Soga, K., & Luo, L. (2018). Distributed fiber optics sensors for civil engineering infrastructure sensing. *Journal of Structural Integrity and Maintenance*, *3*(1), 1–21. doi:10.1080/24705314.2018.1426138

Todd, M. D., Johnson, G. A., & Vohra, S. T. (2001). Deployment of a fiber Bragg grating-based measurement system in a structural health monitoring application. *Smart Materials and Structures*, *10*(3), 534–539. doi:10.1088/0964-1726/10/3/316

Zeng, X., Bao, X., Chhoa, C. Y., Bremner, T. W., Brown, A. W., DeMerchant, M. D., … Georgiades, A. V. (2002). Strain measurement in a concrete beam by use of the Brillouin-scattering-based distributed fiber sensor with single-mode fibers embedded in glass fiber reinforced polymer rods and bonded to steel reinforcing bars. *Applied Optics*, *41*(24), 5105. doi:10.1364/AO.41.005105